

# THE RECENT $H\alpha$ VARIATIONS OF $\zeta$ Tau

Y. NAZÉ<sup>1,2</sup>, J. GUARRO FLO<sup>3</sup>, A. LEDUC<sup>4</sup>, A. STIEWING<sup>5</sup>, S. CURRY<sup>6</sup>, X. DUPONT<sup>7</sup>,

E. BRYSSINCK<sup>8</sup>, H.R. DIZ<sup>9</sup>, E. BERTRAND<sup>10</sup>, C. BUIL<sup>11</sup>, V. DESNOUX<sup>11</sup>, O. GARDE<sup>12</sup>

1) Groupe d’Astrophysique des Hautes Energies, STAR, Université de Liège, B5c, Allée du 6 Août 19c, B-4000 Sart Tilman, Liège, Belgium [ynaze@uliege.be](mailto:ynaze@uliege.be)

2) F.R.S.-FNRS Senior Research Associate

3) Piera Remote Observatory, C. de Jaume Balmes 2, 08784 Piera (Barcelona), Catalonia

4) 18 avenue Shakespeare, 06000 Nice, France

5) 10045 W Royal Oak RD B310, Sun City, AZ 85351, USA

6) SMM Remote Observatory, Av. de Catalunya 38, 25345 Santa Maria de Montmagastrell (Tàrrrega), Catalonia

7) 4 rue de l’Orée du Bois, 37390 Saint-Roch, France

8) BRIXIIS Observatory (MPC B96), Eyckensbeekstraat 2, 9150 Kruikebeke, Belgium

9) Dept of Environmental Science and Engineering, Gannon University, Erie, PA, USA

10) 105 Bd de la côte de beauté, 17640 Vaux Sur Mer, France

11) 13 rue saint-Charles, 75015 Paris, France

12) 2SPOT, 45 Chemin du lac, 38690 Chabons, France

**Abstract:**  $\zeta$  Tau is a well known binary comprising a Be star. Its decretion disk changes with time and we report here on the latest variability behaviour thanks to new amateur data. The cyclic variability observed in the previous years and dominated by the modulated central absorption continues. Only little asymmetries are detected for the  $H\alpha$  line.

## 1 Introduction

$\zeta$  Tau (HD 37202,  $V=3.03$ ) is a bright object of the northern hemisphere. It was observed for centuries and was found to be a binary system a century ago (Adams, 1905). While the main star is a massive star of type B1e, its companion is a low-mass ( $\sim 1 M_{\odot}$ ) object in a 133 d circular orbit (Ruždjak et al., 2009). As in other Be stars,  $\zeta$  Tau harbours a decretion disk whose properties vary over time. In the decade 1997–2008, the  $H\alpha$  line displayed a cyclic behaviour: the profile had a varying central absorption combined to a large modulation between the strengths of the violet and red peaks (known as “V/R” changes). The recurrence time of this cycle was about 1400 d. It was interpreted either as due to a one-armed spiral structure in the disk (Carciofi et al., 2009) or to a precessing disk (Schaefer et al., 2010). Since then, the disk structure has continued to change. Around 2013, the strength of the emission line, evaluated through the equivalent width ( $EW$ ), reached a minimum (Pollmann, 2017). The disk recovered since then, but the cyclic behaviour is not identical to what it was before (Nazé et al., 2022b). Indeed, in 2017–2022, strongly asymmetric profiles were not observed. A varying central absorption depth, however, appeared to drive most of the  $EW$  changes which occurred with a shorter variation timescale (hundreds of days). In this paper, we continue the monitoring of  $\zeta$  Tau

by adding results from two further observing seasons. Section 2 describes the used data, Section 3 provides the results, and Section 4 summarizes and concludes.

## 2 Observations

Because it is a known and bright variable,  $\zeta$  Tau is often a target of amateur observations. Spectra used in this study were downloaded from the collective BeSS database (Neiner et al. 2011 and <http://basebe.obspm.fr>) which gathers such data for thousands of Be stars, making them freely available to the whole astronomical community.

$\zeta$  Tau is observed from August to April each year and 106 spectra were available for the most recent 2022–2023 and 2023–2024 seasons examined in this paper. Each amateur has its own instrument and its own observatory location hence the data were taken in various conditions. The used telescopes, with diameters between 5 and 16 in., were equipped by spectrographs with resolving powers between 9000 and 20 000. Exposure times ranged from 3 to 63 min, usually splitted into several subexposures. All data are of good quality (signal-to-noise ratios of at least 100 in nearly all spectra).

The first reduction steps (bias correction, flat field, wavelength calibration) were performed locally by each amateur in a standard way using various softwares (Audela, ISIS or SpecInti). In addition, a correction for telluric lines contamination was done within IRAF using the template of Hinkle et al. (2000). Normalization was finally performed using low degree polynomials through a chosen set of continuum windows.

Several measurements were done on the line profiles of  $H\alpha$ , after the heliocentric correction was applied (Table 1). First, the  $EW$ s were evaluated from the zero-order moment of the normalized profile, i.e. by doing profile integration between  $-600$  and  $+600$   $\text{km s}^{-1}$ . Second, the depth of the central absorption was measured on each profile. It has a value above 1 if the absorption minimum occurs above the continuum and below 1 otherwise. In a few cases in March 2023, this depth could not be evaluated as the absorption was minimum and the profile complex (multiple peaks) so no value is reported here. Third, Gaussian profiles were fitted to the top of the strongest violet and red peaks. This allowed us to get the amplitudes and positions of these peaks. To ease comparison with literature, we then computed the V/R ratio as in Štefl et al. (2009), i.e. as the ratio of the normalized flux levels of the violet and red peaks, without the usual preliminary correction for the continuum level. For example, if the peaks reach normalized fluxes of 1.6 and 1.4, then V/R is set to  $1.6/1.4=1.14$  not  $0.6/0.4=1.5$ . Finally, radial velocities ( $RV$ s) were determined as in Nazé et al. (2022b). To avoid biases due to the disk changes affecting the central parts of the profile, we focus here on the mirror and double-Gaussians methods (see details in Nazé et al. 2022a). The former method finds the velocity shift at which the the red and blue wings (after reversing the velocities of the blue one) best superimposed (Nemravová et al., 2012). Here, the wings are considered as parts of the profiles with normalized fluxes between 1.16 and 1.50, ensuring minimal contamination by the highly variable line core. The latter method rather finds the velocity shift at which the correlation between the observed profile and a shifted model profile reaches zero (Smith et al., 2012). The model profile consists of two Gaussians with identical widths (here with

standard deviations of  $15 \text{ km s}^{-1}$ ) but opposite amplitudes and centers (here set at  $\pm 1$  and  $\pm 300 \text{ km s}^{-1}$ , respectively). With this choice of parameters, the resulting RVs correspond to bisector velocities at half maximum, with little impact from the varying core.

### 3 Results

Figure 1 shows the line profile variations of the two most recent observing seasons while Figure 2 provides the temporal evolution of the measured line characteristics (from Table 1). The average  $EW$  seems similar to two decades ago: the Be disk has thus recovered from its minimum. As is obvious in the plots, the main change is, again, the varying depth of the central absorption. This is confirmed by the strong correlation between the evolutions of  $EW$ s and absorption depths. The strong line asymmetry observed two decades ago remains absent although small V/R variations can be detected: to give a comparison point, the  $\log(V/R)$  shown in Štefl et al. (2009) varies between  $-0.2$  and  $+0.3$  (i.e. a change in V/R by a factor 3) while here the range is  $-0.04$  to  $+0.07$  (i.e. a change in V/R by 30%). In fact, the profile appears more complex, with multiple subpeaks, when the central absorption is minimum. It may also be noted that the highest peaks appear closer to each other at that time. Finally, when folded on the best-fit ephemeris (Nazé et al., 2022b), the  $RV$ s measured in the new seasons appear in line with the previous ones (Fig. 3).

### 4 Conclusions or Summary

In this paper, we provide measurements characterizing the  $H\alpha$  line associated to the disk of the Be star in  $\zeta$  Tau. The line profile changes continue to be dominated by a central absorption of varying depth. Small asymmetries are detected, but remain far from the strong ones detected two decades ago.

**Acknowledgements:** Y.N. acknowledges support from the Fonds National de la Recherche Scientifique (Belgium), the European Space Agency (ESA) and the Belgian Federal Science Policy Office (BELSPO) in the framework of the PRODEX Programme (contracts linked to XMM-Newton). This work has made use of the ADS, Simbad, and BeSS databases.

### References

- Adams, W. S. 1905, ApJ, 22, 115 [1905ApJ...22..115A](#)
- Carciofi, A. C., Okazaki, A. T., Le Bouquin, J.-B., et al. 2009, A&A, 504, 915 [2009A&A...504..915C](#)
- Hinkle, K., Wallace, L., Valenti, J., & Harmer, D. 2000, Visible and Near Infrared Atlas of the Arcturus Spectrum 3727-9300 A ed. Kenneth Hinkle, Lloyd Wallace,

Table 1: Characteristics of the H $\alpha$  line observed for  $\zeta$  Tau since Spring 2022 (see text for details).

<i>HJD</i> -2.45e6	<i>EW</i> (H $\alpha$ ) ( $\text{\AA}$ )	<i>RV</i> ( $\text{km s}^{-1}$ )		depth	V/R	peak sep. ( $\text{km s}^{-1}$ )	<i>HJD</i> -2.45e6	<i>EW</i> (H $\alpha$ ) ( $\text{\AA}$ )	<i>RV</i> ( $\text{km s}^{-1}$ )		depth	V/R	peak sep. ( $\text{km s}^{-1}$ )
		mirror	2G						mirror	2G			
9819.655	-9.7	13.6	15.1	0.72	0.97	294	10059.622	-13.8	27.3	27.8	1.61	1.02	287
9832.516	-11.4	11.4	11.4	0.98	1.01	307	10171.628	-16.6	25.1	25.2	1.49	1.14	245
9841.684	-14.5	13.3	10.1	1.08	0.99	307	10194.661	-14.6	25.0	29.4	1.60	1.09	270
9875.469	-13.4	15.8	13.7	0.96	1.03	300	10199.617	-15.6	28.4	30.0	1.70	1.10	259
9892.717	-14.6	23.5	24.8	1.07	1.10	283	10206.535	-16.0	23.2	24.3	1.76	1.08	233
9894.423	-14.7	25.9	26.6	1.08	1.11	277	10212.548	-14.5	23.9	24.3	1.67	1.06	228
9900.393	-14.7	22.9	27.5	1.07	1.16	271	10220.594	-14.4	20.7	22.8	1.62	1.10	219
9902.445	-15.0	22.2	26.9	1.07	1.14	272	10225.649	-14.9	16.7	18.7	1.66	1.08	201
9903.435	-14.4	25.9	29.8	1.06	1.15	272	10229.457	-14.3	19.5	20.6	1.63	1.05	272
9907.677	-15.0	25.4	27.5	1.19	1.17	260	10238.533	-14.8	12.0	13.6	1.62	1.06	270
9909.385	-14.6	26.1	27.3	1.21	1.16	258	10247.497	-14.1	9.1	10.4	1.56	1.04	285
9909.407	-15.0	24.4	27.1	1.22	1.15	260	10250.855	-14.6	10.4	11.4	1.56	1.00	291
9910.404	-15.3	27.8	29.8	1.25	1.14	258	10255.490	-14.2	10.9	12.5	1.53	1.03	289
9915.355	-15.4	26.1	26.7	1.36	1.14	235	10261.443	-14.4	10.8	11.9	1.41	1.03	287
9925.409	-17.6	27.1	32.6	1.61	1.01	260	10261.510	-14.0	11.3	11.9	1.39	1.04	288
9931.424	-18.0	24.2	25.7	1.90	1.02	268	10264.386	-14.7	9.1	9.8	1.41	1.03	287
9932.407	-17.0	26.7	27.8	1.87	0.99	245	10266.416	-14.2	8.8	9.4	1.37	1.03	288
9934.633	-15.6	29.0	31.3	1.78	0.96	229	10267.490	-13.4	9.8	11.6	1.34	1.01	289
9940.475	-18.3	23.7	26.7	1.99	0.97	227	10268.443	-14.3	10.7	14.5	1.35	1.01	288
9958.435	-18.8	19.8	20.4	2.12	0.92	197	10270.487	-14.0	14.1	15.3	1.32	1.01	289
9962.304	-19.8	16.1	19.1	2.26	0.92	182	10272.490	-13.2	13.4	14.6	1.28	1.02	286
9972.640	-19.8	8.9	13.1	2.42	0.92	145	10277.383	-13.6	18.4	24.2	1.27	1.02	286
9983.614	-19.5	-3.4	3.2	2.46	1.02	137	10277.396	-13.7	15.3	20.4	1.24	1.02	287
9987.643	-19.9	10.4	11.9	2.44	0.99	151	10281.434	-13.1	21.4	21.5	1.20	1.01	284
9995.439	-19.8	12.3	13.8	2.48	0.94	133	10281.498	-13.1	19.3	23.7	1.23	1.01	284
9996.362	-19.1	12.7	13.7	2.37	0.94	139	10285.504	-14.8	22.1	25.7	1.24	1.03	284
10003.351	-17.9	9.9	10.5	2.25	0.95	134	10287.465	-14.0	15.8	16.1	1.19	1.07	277
10008.382	-18.0	17.2	17.8				10288.575	-13.9	24.3	26.1	1.18	1.05	287
10009.306	-18.3	14.9	17.2				10293.474	-13.6	18.4	21.5	1.18	1.08	279
10010.301	-18.9	12.1	13.5				10294.521	-14.2	24.3	24.6	1.20	1.09	284
10011.345	-18.3	17.4	19.2				10295.462	-13.7	17.4	20.3	1.19	1.09	282
10012.406	-18.0	20.4	22.3				10296.350	-14.8	23.2	26.2	1.20	1.09	285
10013.376	-18.3	14.4	15.6				10296.391	-14.2	25.3	28.2	1.17	1.09	289
10014.323	-17.7	15.3	17.2				10296.396	-14.0	18.2	22.6	1.15	1.09	285
10015.321	-17.2	19.8	21.5				10299.332	-15.7	20.8	22.8	1.24	1.12	283
10016.301	-17.3	14.6	17.2				10302.431	-14.8	22.5	24.2	1.18	1.10	283
10018.388	-17.0	20.3	19.9				10304.417	-13.8	23.0	25.4	1.19	1.09	302
10019.330	-16.9	21.0	21.2	2.10	0.93	211	10306.389	-14.5	22.7	22.8	1.20	1.09	283
10020.406	-17.6	17.6	20.0	2.17	0.93	207	10309.511	-13.7	23.6	27.4	1.12	1.10	282
10020.644	-16.8	18.7	21.0	2.09	0.93	209	10311.467	-13.8	27.2	28.6	1.12	1.10	291
10021.326	-16.8	18.3	21.2	2.09	0.91	206	10316.700	-14.1	20.3	22.4	1.09	1.10	287
10023.320	-17.0	18.8	20.4	2.10	0.93	202	10317.355	-13.3	24.9	27.5	1.04	1.09	297
10024.319	-17.0	19.1	19.7	2.10	0.94	204	10318.488	-13.6	24.4	27.5	1.07	1.10	298
10028.306	-16.5	15.9	16.6	2.06	0.96	196	10321.268	-13.9	25.1	29.0	0.99	1.09	294
10028.708	-17.0	18.0	19.3	2.08	0.95	199	10326.588	-12.5	18.5	20.9	0.90	1.10	296
10029.310	-15.9	19.7	20.7	2.03	0.96	197	10327.499	-12.9	24.4	28.5	0.95	1.06	291
10031.326	-16.7	22.8	23.4	2.07	0.97	202	10328.269	-13.7	25.7	28.3	0.95	1.08	296
10032.344	-16.7	21.6	21.8	2.10	0.99	198	10328.417	-13.7	27.1	30.2	0.95	1.08	299
10033.342	-16.6	17.0	19.4	2.06	0.99	193	10331.248	-14.0	21.4	23.9	0.99	1.09	291
10034.564	-16.8	7.7	16.2	2.06	1.02	187	10335.255	-13.6	23.3	24.9	0.92	1.09	286
10037.313	-16.4	16.5	17.4	2.08	1.00	164	10337.262	-13.9	20.3	20.6	0.94	1.11	290
10039.566	-16.9	12.3	18.5	2.05	1.01	176	10339.577	-14.1	21.5	25.3	1.03	1.09	283
10040.611	-15.0	22.9	22.7	1.97	1.03	146	10342.384	-14.2	18.5	21.6	1.14	1.07	277

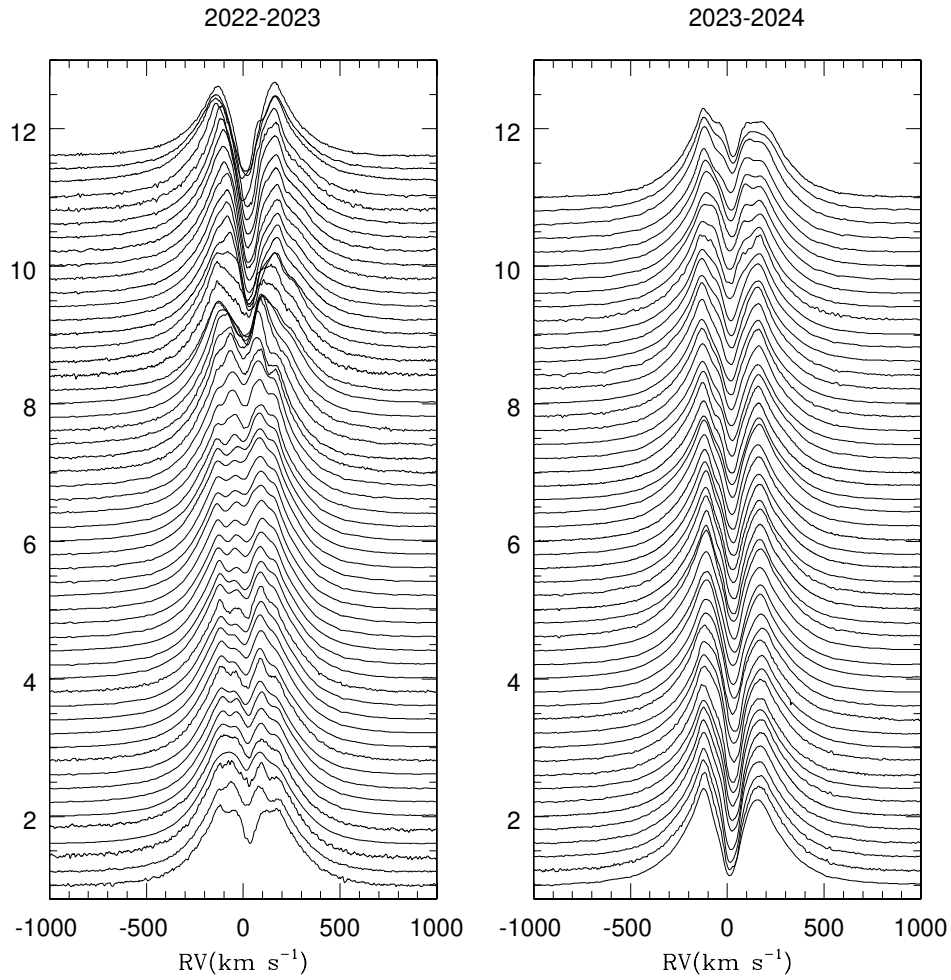


Figure 1: Evolution of the H $\alpha$  line profile of  $\zeta$  Tau over two observing seasons. Time is running downwards.

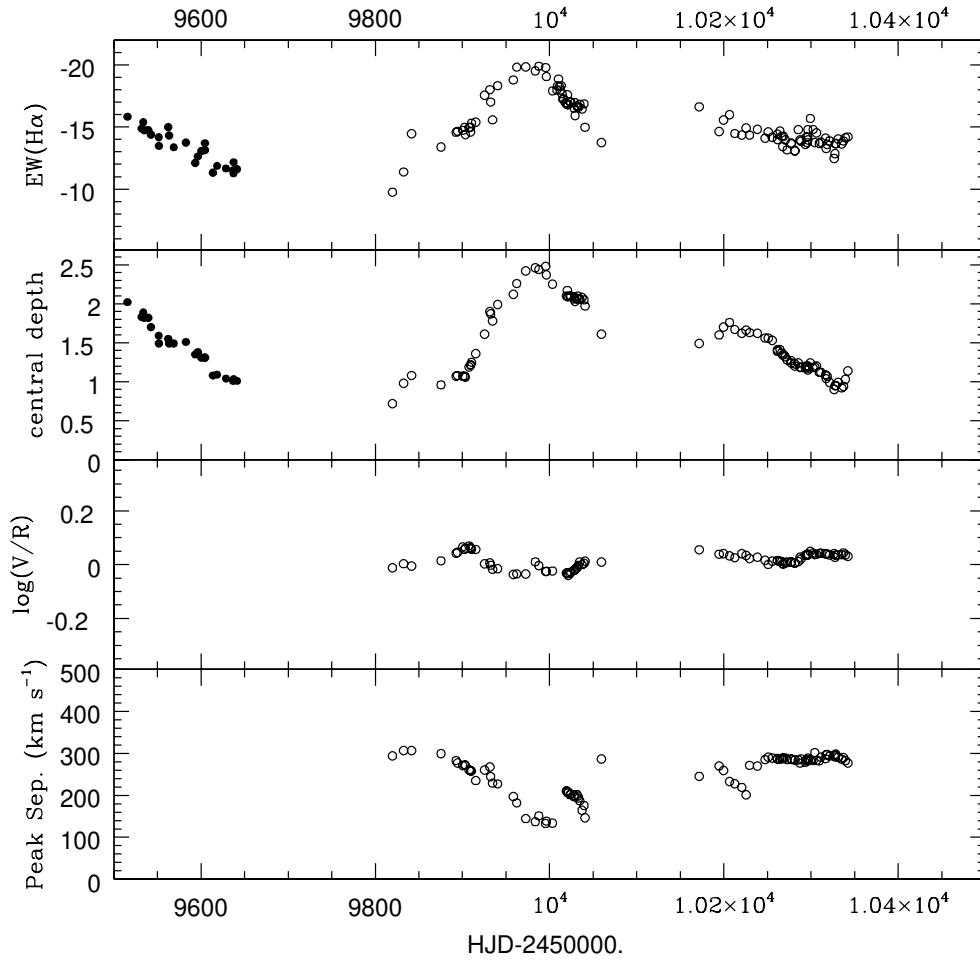


Figure 2: Evolution with time of several characteristics of the  $H\alpha$  line in  $\zeta$  Tau:  $EW$ s, depth of the central absorption,  $V/R$ , and separation between the highest violet and red peaks. Black dots on the left correspond to values reported in Nazé et al. (2022b).

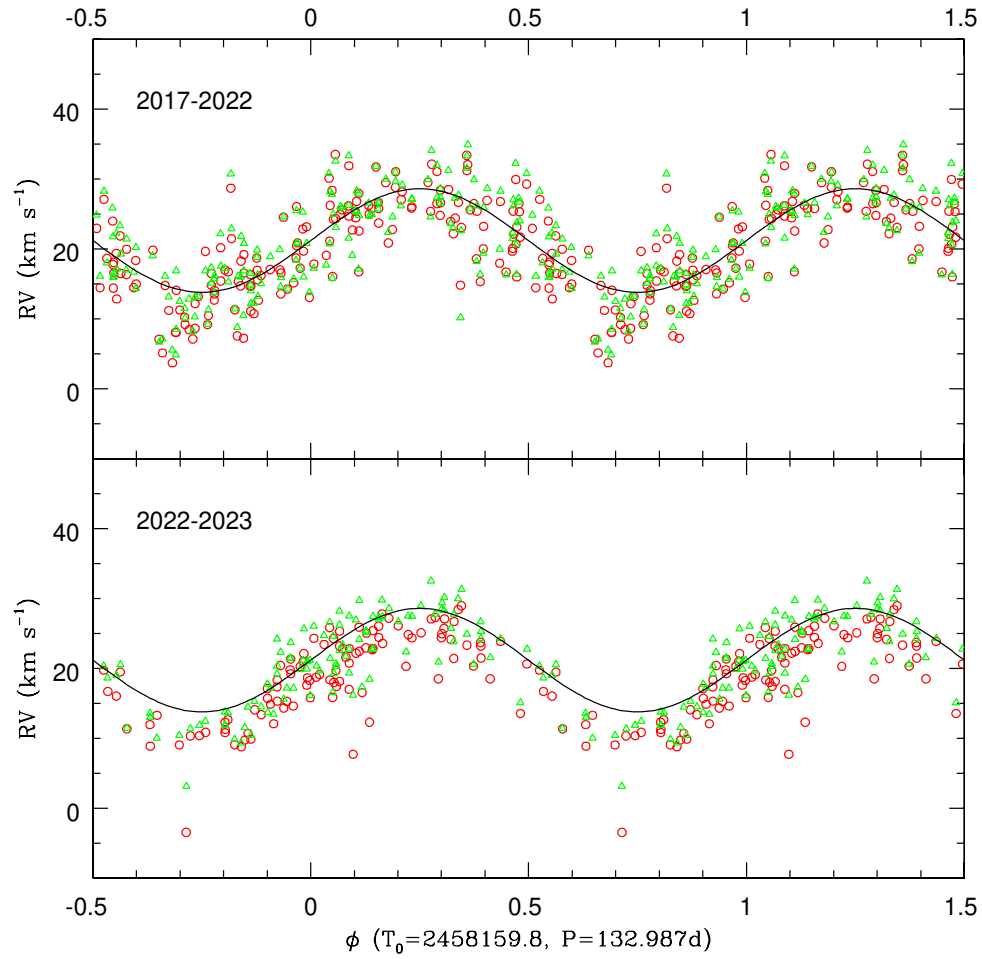


Figure 3:  $RV$ s of the  $H\alpha$  line derived for  $\zeta$  Tau using the mirror method (red circles) or the double-Gaussian method (green triangles), folded with the best-fit ephemeris of Nazé et al. (2022b). Top panel shows the  $RV$ s reported in Nazé et al. (2022b) for seasons 2017–2022, and bottom panel the new data (2022–2024). The best-fit sinusoid from Nazé et al. (2022b) is superimposed to both panels.

- Jeff Valenti, and Dianne Harmer. (San Francisco: ASP) ISBN: 1-58381-037-4, 2000. [2000vnia.book.....H](#)
- Nazé, Y., Rauw, G., Czesla, S., et al. 2022a, MNRAS, 510, 2286 [2022MNRAS.510.2286N](#)
- Nazé, Y., Rauw, G., Smith, M. A., et al. 2022b, MNRAS, 516, 3366 [2022MNRAS.516.3366N](#)
- Neiner, C., de Batz, B., Cochard, F., et al. 2011, AJ, 142, 149 [2011AJ....142..149N](#)
- Nemravová, J., Harmanec, P., Koubský, P., et al. 2012, A&A, 537, A59 [2012A&A...537A..59N](#)
- Pollmann, E. 2017, Information Bulletin on Variable Stars, 6208 [2017IBVS.6208....1P](#)
- Ruždjak, D., Božić, H., Harmanec, P., et al. 2009, A&A, 506, 1319 [2009A&A...506.1319R](#)
- Schaefer, G. H., Gies, D. R., Monnier, J. D., et al. 2010, AJ, 140, 1838. [2010AJ....140.1838S](#)
- Smith, M. A., Lopes de Oliveira, R., Motch, C., et al. 2012, A&A, 540, A53 [2012A&A...540A..53S](#)
- Štefl, S., Rivinius, T., Carciofi, A. C., et al. 2009, A&A, 504, 929 [2009A&A...504..929S](#)